

# PROCEEDINGS OF SPIE

[SPIDigitalLibrary.org/conference-proceedings-of-spie](https://spiedigitallibrary.org/conference-proceedings-of-spie)

## Experimental phase-error extraction and modelling in silicon photonic arrayed waveguide gratings

Khan, Umar, Fiers, Martin, Bogaerts, Wim

Umar Khan, Martin Fiers, Wim Bogaerts, "Experimental phase-error extraction and modelling in silicon photonic arrayed waveguide gratings," Proc. SPIE 11285, Silicon Photonics XV, 1128510 (26 February 2020); doi: 10.1117/12.2544645

**SPIE.**

Event: SPIE OPTO, 2020, San Francisco, California, United States

# Experimental phase-error extraction and modelling in silicon photonic arrayed waveguide gratings

Umar Khan<sup>a</sup>, Martin Fiers<sup>b</sup>, Yufei Xing<sup>a</sup>, and Wim Bogaerts<sup>a</sup>

<sup>a</sup>Ghent University - IMEC, Photonics Research Group, Department of Information Technology,, Technologiemark-Zwijnaarde 126, 9052 Gent, Belgium

<sup>b</sup>Luceda Photonics, Noordlaan 21, 9200 Dendermonde, Belgium

## ABSTRACT

We present a detailed study of parameter sweeps of silicon photonic arrayed waveguide gratings (AWG), looking into the effects of phase errors in the delay lines, which are induced by fabrication variation. We fabricated AWGs with 8 wavelength channels spaced 200 GHz and 400 GHz apart. We swept the waveguide width of the delay lines, and also performed a sweep where we introduced increments of length to the waveguides to emulate different AWG layouts and look into the effect of the phase errors. With this more detailed study we could quantitatively confirm the results of earlier studies, showing the wider waveguides reduce the effect of phase errors and dramatically improve the performance of the AWGs in terms of insertion loss and crosstalk. We also looked into the effect of rotating the layout of the circuit on the mask, and here we could show that, contrary to results with older technologies, this no longer has an effect on the current generation of devices.

**Keywords:** Arrayed Waveguide Gratings, Silicon Photonics

## 1. INTRODUCTION

Silicon photonics is undoubtedly becoming an increasingly prominent technology for *photonic integrated circuits* (PICs) with the application base expanding from optical communications to sensing.<sup>1</sup> There are two main contributing factors in this success i.e. use of the existing *complementary metal oxide semiconductor* (CMOS) infrastructure for manufacturing and the high material index contrast between the guiding silicon and the cladding which allows for sub-micron waveguides and a high integration density. However, this advantage of having a high index contrast has a downside also, i.e. devices become very sensitive to the geometry variations and which degrades device and circuit performance. For example, deviation from the designed waveguide geometry will severely shift the spectrum of a waveguide-based filter device, in the order of 1 nm wavelength shift for a 1 nm change in dimensions.<sup>2</sup> Device performance degradation propagates and accumulates to the circuit level and can rapidly decrease the yield of large circuits, i.e., the number of fabricated circuits working as intended. Ultimately this leads to an increase in the cost of the delivered product.

In this paper, we discuss the effect of fabrication imperfections on the performance of *arrayed waveguide grating* (AWG) devices after providing an insight into the fabrication variability. Since the 1990s, AWGs have been a key component in communication systems using wavelength division multiplexing, as they provide an elegant mechanism to combine, separate and route a large number of wavelength channels in a single device, with good uniformity and low crosstalk.<sup>3,4</sup> In high-contrast silicon photonics, AWGs have never scaled up to the channel count and performance of technologies with a much lower index contrast: while the waveguides are more compact and reduce the footprint of the AWG, the sensitivity to imperfections and variations invariably limits the scaling of these devices.

---

Further author information: (Send correspondence to W.B.)

W.B.: E-mail: wim.bogaerts@UGent.be, Telephone: 32 9 264 3324

## 2. ARRAYED WAVEGUIDE GRATINGS (AWGS)

An AWG consists of an array of waveguides placed between two free-space focusing regions called star couplers.<sup>3-5</sup> An example of an SOI-based 8-channel (400 GHz channel spacing) AWG device is shown in Fig. 1(a) below. Light entering the input star coupler diverges and gets coupled to the waveguide array. The length difference between the waveguides,  $\Delta L$ , is designed such that their optical path length difference equals an integral multiple of the central wavelength,  $\Delta L = m\lambda_c/n_{eff}$ . In the output star coupler, light at that wavelength will arrive in phase and is focused in the center of the image plane, where it can be collected by a waveguide aperture. As the wavelength moves away from  $\lambda_c$ , the focus shifts along the image plane. Output waveguides are placed along this image plane, each capturing a different section of the spatially separated spectrum.

AWGs are considered to be the key devices for for *wavelength division multiplexing* (WDM) systems because of their capability for simultaneously filtering out multiple wavelengths from a broadband input. AWG devices are mostly used for multiplexing/demultiplexing and routing in WDM optical communication, but today they are also explored as wavelength filters or spectrometers in lab-on-a-chip based systems for photonic sensing and spectroscopy, and even in optical beamsteering applications.<sup>6-9</sup> Typical figures of merit to characterize AWG devices are the *insertion loss* (IL), *cross-talk* (XT), *next-neighbour crosstalk* (NNXT) and center wavelength ( $\lambda_c$ ). An example of a measured transmission spectrum for an 8-channel AWG with 400 GHz channel spacing is shown in Fig. 1(b).

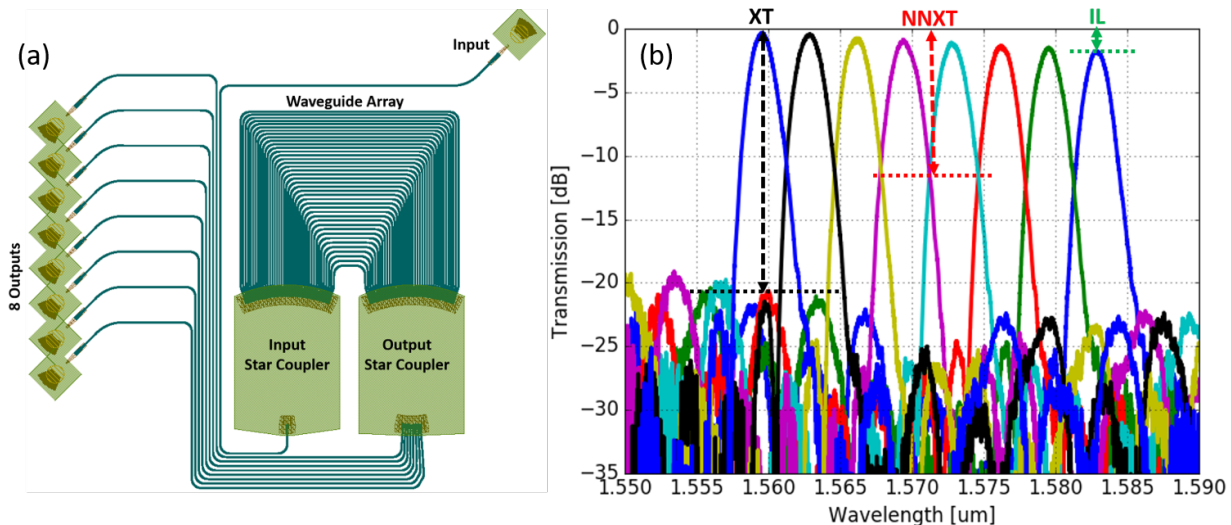


Figure 1. (a) An AWG device with 8 output channels, designed for imec's iSiPP50G platform.<sup>10</sup> Optical ports, input and output star couplers and the waveguide array are clearly marked. This AWG device is designed to have the output channel wavelengths spaced 400 GHz (3.2 nm) apart. (b) Measured transmission response from 8 outputs of the device. Crosstalk (XT), next-neighbour crosstalk (NNXT) and insertion loss (IL) are marked in the plot. The transmission is normalized to the transmission spectrum of a straight waveguide, so some variations in insertion loss can be attributed to variability of the grating couples used for coupling the light from fiber to chip and back.

The performance of an AWG, which translates in low insertion loss and crosstalk, is determined by how well the input waveguide aperture is imaged onto the image plane at the output and can be captured by the waveguide apertures placed there. The high contrast of submicrometer silicon photonics greatly helps to confine light into small volumes, but it plays a detrimental role in various parts of the AWG. First of all, when a waveguide transitions into the free propagation region in the star coupler, there is a discontinuity which can cause unwanted scattering and reflections, which in turn could interfere with other channels. Also, the high contrast discontinuity induces a discontinuity in the electric field of the waveguide mode: This discontinuity is very hard to reproduce with converging beams at the image plane, which limits the modal overlap and therefore the power transmission to the output waveguide. Reducing the abruptness of these discontinuities using a partial etch<sup>11,12</sup> or using subwavelength gratings<sup>13</sup> significantly reduces this effect, but it does not completely eliminate

it. A second effect in high-contrast waveguides which deteriorates the image quality is the accumulation of phase errors in the delay line. Even nanometer-scale geometry variations in high-contrast waveguides can induce non-negligible changes in the effective index of the waveguide, changing the optical path length.<sup>14</sup> This has been addressed using different techniques. Rather than using AWG delay lines with variable curvature, the common practice in silicon photonics is to orient the delay lines along the X and Y direction.<sup>11</sup> This reduces the impact of a radius-dependent effective index, and also reduces the unknown contribution of bend discretisation. A second improvement is to use wider waveguides in the straight sections of the delay line.<sup>11,12</sup> As wider waveguides have a higher mode confinement and lower optical intensity on the sidewalls,<sup>15</sup> the sensitivity to random width variations is reduced, and this reduces the phase errors. Other effects that can affect the optical path length of the waveguide is mask discretisation:<sup>16</sup> moving from a 5 nm grid to a 1 nm grid can result in a considerable improvement.

With this sensitivity, we expect that the performance of AWGs will suffer when the delay lines become too long, as this will accumulate progressively more phase errors.<sup>14</sup> The length of the delay  $\Delta L$  is directly determined by the channel spacing and the number of wavelength channels. On top of that, when the channel count increases, more delay lines are needed to provide good imaging in the image plane. This results in a longer average delay, again adding to the phase errors. Overall, we find that with the current state of the technology, silicon photonics AWGs are mostly suited for applications where the channel count is limited (<64) and the channel spacing is not too small (>100 GHz). Also, the channel spacing cannot be made arbitrarily large, because then the delay lines would be spaced too close together, and alternative layouts are needed which typically induce more phase errors.<sup>17</sup>

### 3. FABRICATION VARIABILITY

Fabrication variability covers all variations from the designed circuit induced by the chip fabrication process, and which are not identical for all copies of the circuit on the die or wafer. Most relevant to our work, it induces an undesirable position-dependent change in linewidth and thickness of the photonic waveguides. Different process conditions like exposure dose, plasma density, resist age and *chemical mechanical polishing* (CMP) slurry composition lead to variations in the linewidth, layer thickness, sidewall angles, gap between waveguides and doping profile.<sup>18–20</sup> These variations can have different distributions over the wafer. Fabrication variability is present at different levels e.g. lot-to-lot, wafer-to-wafer, die-to-die and device-to-device and can be environmental, temporal or spatial.<sup>21</sup> Environmental and temporal variabilities are usually reflected at the wafer-to-wafer and lot-to-lot level and they are not the main focus of this research. The spatial variability is the core of this research as it affects the device performance and is dependent on the distance between devices or device's location on the wafer. As already mentioned, a silicon wire waveguide is very sensitive to change in linewidth and thickness, and therefore its optical properties (e.g. the effective and the group indices) change as the geometry of the waveguide changes. This change in optical properties can lead to phase errors in interferometric circuits with multiple delay lines (such as the AWG under study), even when waveguides are placed close together. Often, elements closer together are more likely to have less variability than the elements further apart. The sensitivity to nanometer-scale variations in a submicron *silicon-on-insulator* (SOI) platform is generally not acceptable for a lot of applications using *dense wavelength division multiplexing* (DWDM).<sup>1</sup>

### 4. EFFECT OF FABRICATION VARIABILITY ON AWGS

High index contrast platforms such as SOI can be used to realize very compact AWG devices. The downside is that these devices become very sensitive to variations in geometry of the waveguides. Side wall roughness and width variations of the waveguides are considered to be the main contributions in introducing the phase errors in the delay lines which result into enhanced cross-talk between the output channels of the AWGs.<sup>22</sup> To quantitatively analyze the effect of fabrication imperfections we designed and fabricated variations of 8-channel AWGs with different variations:

- Two different channel spacings: We designed AWGs with 400 GHz (3.2 nm) and 200 GHz (1.6 nm) channel spacing. All other aspects being the same, the smaller channel spacing doubles the delay difference between the arms of the AWG, resulting in larger phase errors.

- Additional length in the delay lines: Here we (unnecessarily) add length to all delay lines (while keeping the other specs fixed), effectively increasing the phase errors. This gives a more direct comparison of the effect of waveguide length, compared to the earlier study done in.<sup>23</sup>
- Waveguide width: We did a comprehensive sweep of the waveguide width for identical design parameters, looking at the incremental improvements in performance that we can get beyond the results published in.<sup>12</sup>
- Rotating the AWGs: It was reported in<sup>24</sup> that rotating the same AWG design away from the X or Y direction had a detrimental effect. As this was reported many years ago in a currently outdated technology, we wanted to see how the device rotation has an impact on today's technology platform.

The AWG devices were designed and simulated using Luceda Photonics' dedicated filter toolbox algorithms. The simulation involves a combination of eigenmode expansion, semi-analytical Fresnel diffraction and a circuit model with stochastic phase errors.<sup>25</sup> The layouts were generated on a 1 nm mask grid to reduce variations due to mask discretisations<sup>16</sup> and fabricated on imec's PSV iSiPP platform through the Europractice *multi-project wafer* (MPW) service. The fabricated AWG devices over a wafer were measured using a tunable laser and a photodetector in a clean-room environment using a wafer-scale automated alignment tool.

#### 4.1 Extra length of waveguides

We designed AWG devices with a rectangular layout for the delay lines, adding additional length along one direction. We used 7 different extra lengths ranging from 50  $\mu\text{m}$  to 1200  $\mu\text{m}$ , and the width of the delay lines (waveguides) was fixed at 450 nm to get a quantitative insight in the effect of phase errors which are proportional to  $\sqrt{L}$ .<sup>14</sup> We choose this width of 450 nm rather than a wider width in order to better observe the length statistics of the phase errors. The sketch in Fig. 2(a) explains how extra lengths are being added to the AWG devices. AWG devices having different extra lengths can be noticed in the microscope image in Fig. 2(b). The additional length in all the arms does not affect the ideal behavior of the device, but will increase the effect of phase errors. The effect of the extra lengths on the *insertion loss* (IL), *cross-talk* (XT) and the *next-neighbor cross-talk* (NNXT) is shown in Fig. 2(c). It can be noticed in the graph that the extinction ratio decreases (the difference between the blue line and the red/green lines) with increasing extra lengths in the delay lines. The two main contributions here are the side wall roughness and the local variability. Local variability results in changes of the waveguide width along the length of the waveguides and between adjacent waveguides, causing a phase mismatch at the outputs of the arms. This phase mismatch results in a ripple of the phase front as it propagates into the second star coupler. The result is an imperfect field profile in the image plane resulting in lower coupling to the waveguide and coupling to the other waveguide apertures. As a result, this lowers the extinction ratio (higher cross-talk). In this reasoning, we are assuming the thickness of the waveguides to be constant as thickness variation is a wafer-level slowly varying phenomenon.

The extracted insertion loss and cross-talks for different extra lengths are plotted in Fig. 3 for detailed analysis. It can clearly be noticed in the plots that insertion loss increases with increasing lengths. Measurements show increase in insertion loss from around 3 dB for an extra length of 50  $\mu\text{m}$  to almost 10 dB for extra length of 1200  $\mu\text{m}$ . Phase errors due to longer lengths of the waveguides are considered to be the biggest contributors in this loss increase, although we can expect a small loss due to the longer propagation length through the waveguides, which have a propagation loss of  $\approx 2\text{dB/cm}$ . As expected, the extinction ratio decreases with increasing length of the delay lines due to the local variability. So, addition of the lengths into the waveguides should be avoided for optimal performance of the AWG devices. While in these devices the extra length was artificially added, it can also be a result from a different layout, such as the S-shaped AWG layouts that are needed when the delay length  $\Delta L$  becomes too short.<sup>17</sup> For the other parameter sweeps, we kept the extra length to zero.

#### 4.2 Width of the waveguides

It has already been proven that increasing the width of the delay lines reduces the phase errors, with a dramatic improvement in the performance of the AWG.<sup>11,12</sup> Here we want to quantitatively assess these improvements for different widths. The widths of the delay lines were varied in 12 steps from 0.3  $\mu\text{m}$  to 1.2  $\mu\text{m}$  for AWGs with zero extra length (EL = 0  $\mu\text{m}$ ). The implementation of this variation is explained in Fig. 4(a). It can be noticed that

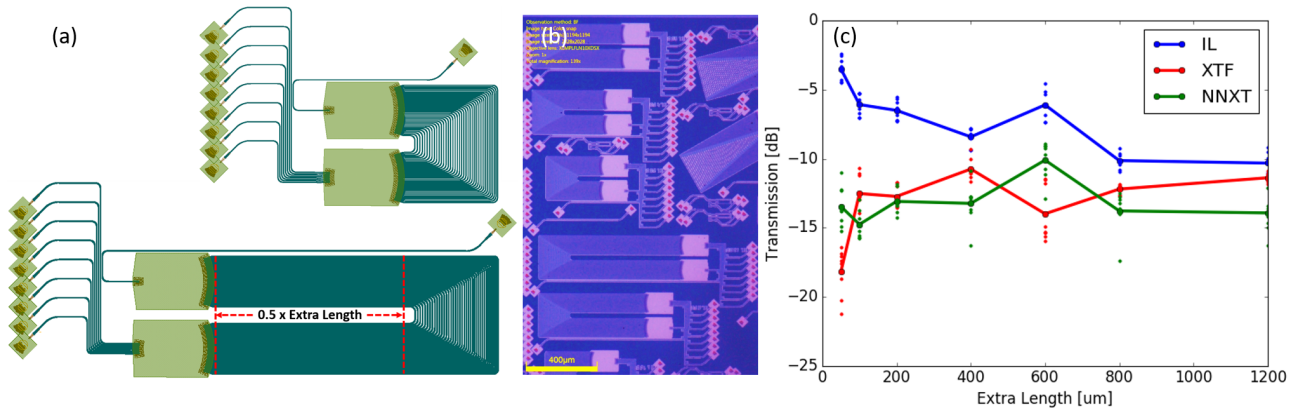


Figure 2. (a) A snippet from the GDSII mask layout file of an AWG with 400 GHz channel spacing, explaining the addition of extra length in the waveguide array. (b) Microscope image of the devices having different extra lengths. (c) The plot shows that insertion loss of the AWG devices increases with increasing extra lengths. The extinction ratio decreases with increasing extra lengths.

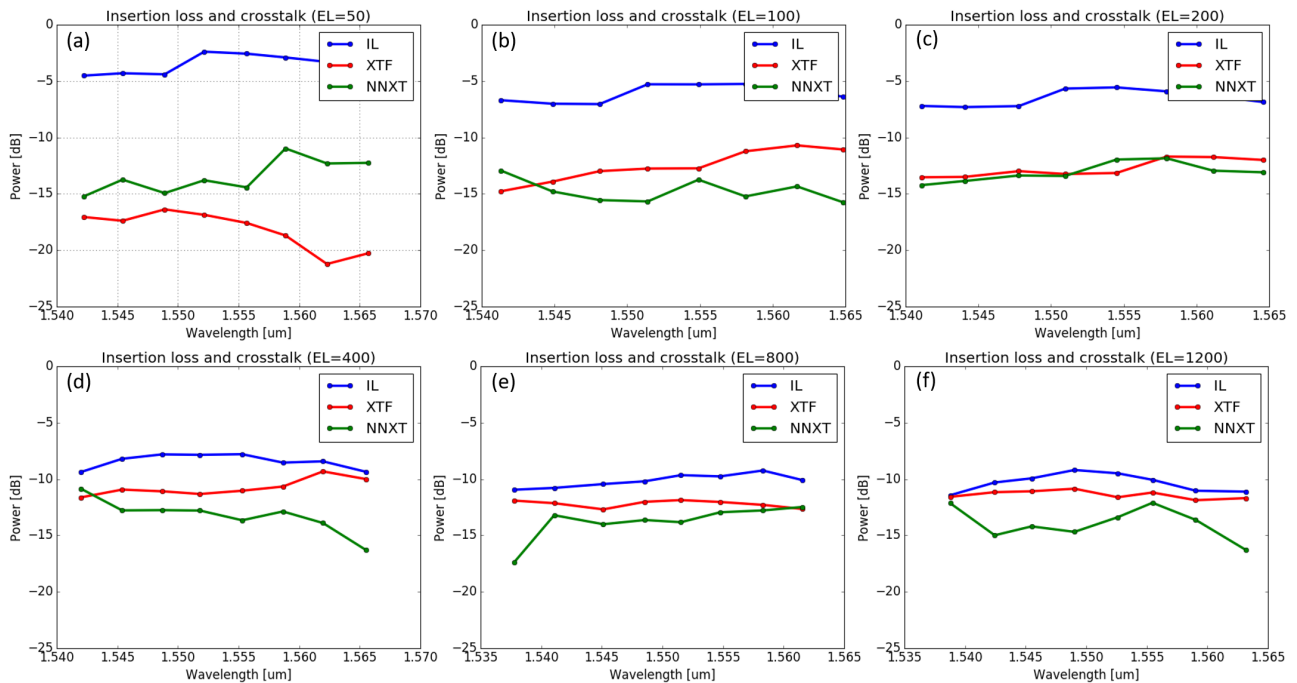


Figure 3. Experimentally extracted *insertion loss* (IL), *cross-talk* (XTF) and *next-neighbour crosstalk* (NNXT) values for AWG devices having extra lengths (EL) (a) 50  $\mu\text{m}$  (b) 100  $\mu\text{m}$  (c) 200  $\mu\text{m}$  (d) 400  $\mu\text{m}$  (e) 800  $\mu\text{m}$  and (f) 1200  $\mu\text{m}$ .

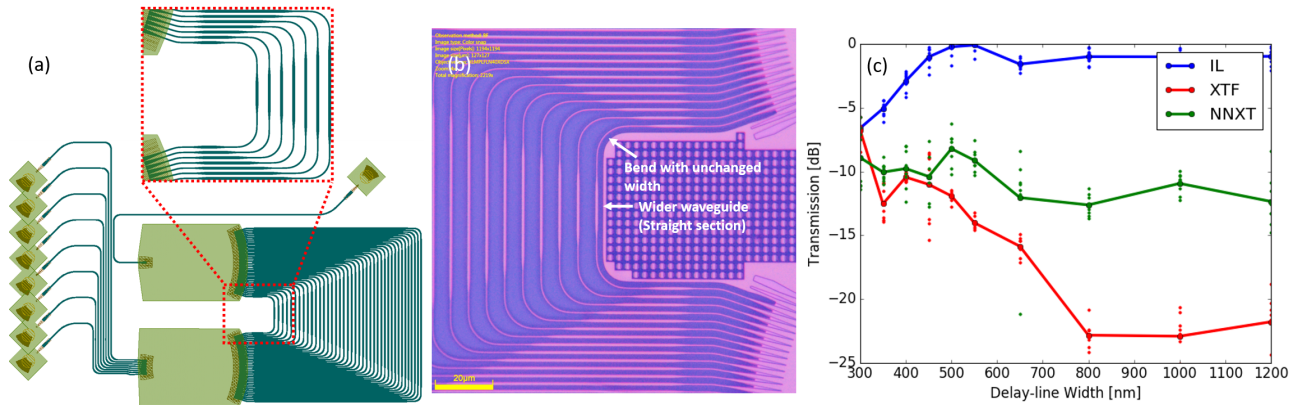


Figure 4. (a) A snippet from the GDSII file explaining the variation in widths of the waveguides in the waveguide array of an AWG device. It should be noticed here that width of the waveguides at the bends is not varied to make sure that higher order modes are not being generated in the bending regions. (b) Microscope image showing that width of the waveguide is not changed in the bends. The width is changed only in the straight sections. (c) Experimentally extracted insertion loss (IL), crosstalk (XTF) and next-neighbour crosstalk (NNXT) values for devices with different waveguide widths of the delay lines.

width of the waveguides in the bends is kept at 450 nm to make sure that higher order modes are not generated in these bend sections. This means that we have two types of waveguides in each delay line, connected by tapers. We designed those lengths such that the increment  $\Delta L$  is always in the waveguides with a different width, and all delay lines have the same length of 450 nm wide segments. Also, the actual delay length  $\Delta L$  is adjusted for the different value of the effective index  $n_{eff}$ , to obtain the same FSR and channel spacing for all devices.

The *insertion loss* (IL), *cross-talk* (XT) and the *next neighbor cross-talk* (NNXT) for the devices with varying width of the delay lines are shown in Fig. 4(c). It can be noticed that the extinction ratio increases (cross-talk decreases) with increasing waveguide widths.

The extracted insertion loss and cross-talks for different widths of the waveguides in the delay lines are plotted in Fig. 5 for detailed analysis. It can clearly be noticed in the plots that insertion loss decreases with increasing width. Measurements show improvement in insertion loss from almost 5 dB to almost 0 dB when we increase the widths of the straight section from 350 nm (narrower than the standard 450 nm) to 1200 nm respectively. Calculated fundamental TE modes for 450 nm and 800 nm wide waveguides are shown in Fig. 5(d) and (h) respectively. It can be noticed from the calculated mode profiles that less of the mode interacts with the side walls as the waveguide gets wider. This weaker interaction has a positive effect on the insertion loss as sidewall roughness plays less of a role. Also, the crosstalk can be found to improve with increasing width of the waveguides. As the waveguide gets wider, small variations in waveguide width (also related to the side walls) cause less of a variation in the local  $n_{eff}$ , because the light is more confined.

Figure 6 shows the transmission spectra of the 8 channels for AWGs with different widths. Indeed, we can visually confirm the trend from Fig. 5 and Fig. 4 that the performance gets better with wide width. But it is also clear that the channels are not properly aligned at the same wavelengths. This can be attributed to a systematic deviation of the fabricated waveguides from the designed dimensions, which results in a different value of the effective index  $n_{eff}(w, \lambda)$ . In Fig. 6(f) we plot the original model which we used for the design versus the extracted value from the measurements.

### 4.3 Rotation of the devices

The common design practice for AWGs in submicrometer high-contrast waveguides is to orient the delays as much as possible along the X and Y directions that correspond with the grid of the mask file format. This is possible in such high-contrast waveguides because the bend radius can be reduced to a few micrometers. The preference for X or Y orientation was confirmed in early experiments in.<sup>24</sup> There, it was observed that the performance (IL, XT) of AWG devices degrades if identical devices are rotated at different angles.<sup>24</sup> Rotations

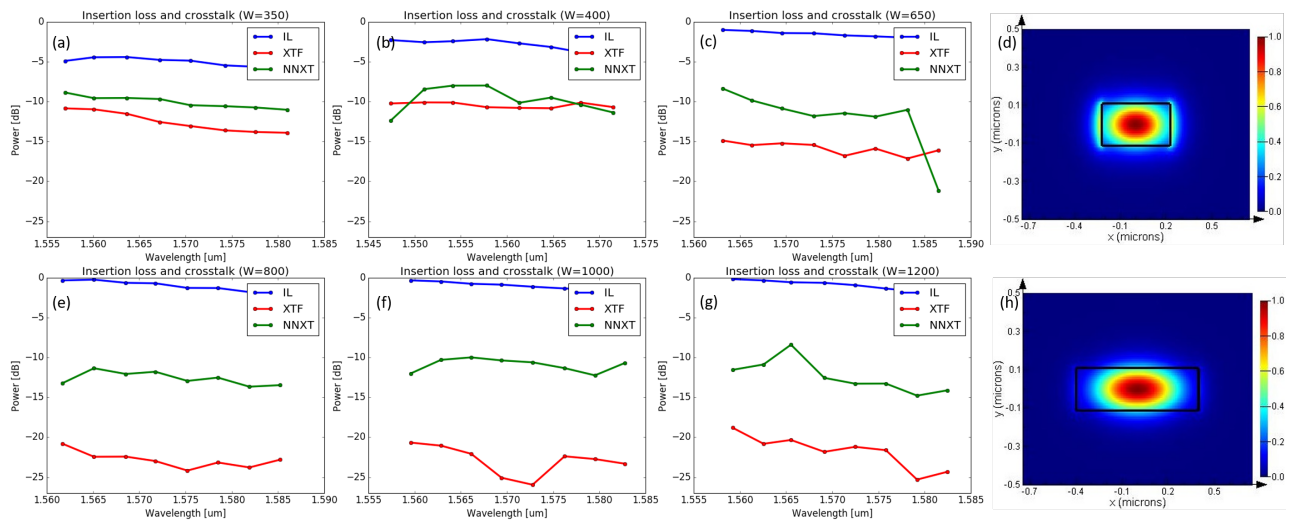


Figure 5. Experimentally extracted insertion loss (IL), cross-talk (XTF) and next-neighbour crosstalk (NNXT) values for AWG devices having waveguide widths of (a) 350 nm (b) 400 nm (c) 650 nm (e) 800 nm (f) 1000 nm and (g) 1200 nm. Calculated fundamental TE modes for 450 nm and 800nm waveguides are shown in (d) and (h) respectively.

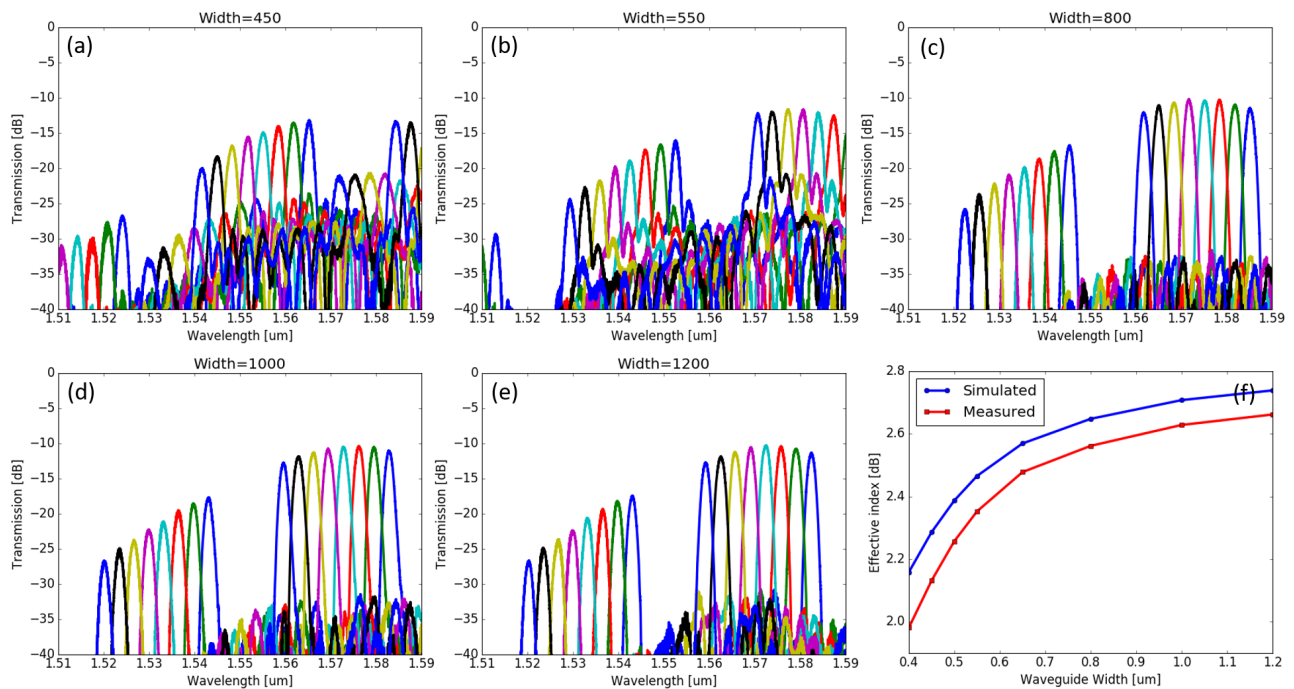


Figure 6. (a) Measured transmission responses for waveguide widths of (a) 450 nm (b) 550 nm (c) 800 nm (d) 1000 nm and (e) 1200 nm. (f) A comparison between the simulated and experimentally extracted refractive index values.

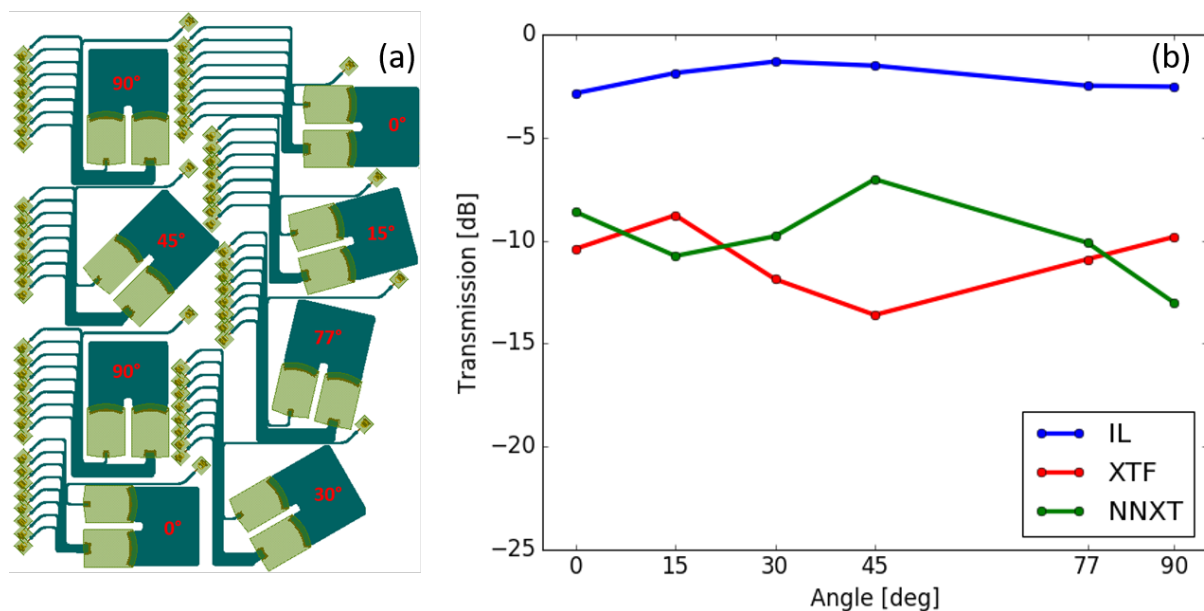


Figure 7. (a) A snippet from the GDSII explaining the rotation of the AWG devices at different angles. You can notice two devices each for  $0^\circ$  and  $90^\circ$  rotations. (b) Experimentally extracted *insertion loss* (IL), *crosstalk* (XTF) and *next-neighbour crosstalk* (NNXT) values for devices with different rotations.

at  $0^\circ$  and  $90^\circ$  showed little difference. But when rotated at  $45^\circ$ , the crosstalk increased, and this became worse for more irregular angles. At that time, the cause of these degradations was attributed to the discretization during the processing of the mask file, and the mask writing strategy. These reported results used a technology platform at imec which is no longer in use, based on 248 nm lithography with a 5 nm mask grid.

We tried to reproduce this on today's technology based on 193 nm lithography with a 1 nm mask grid. In order to find out the effect of mask discretization on AWG devices, 8-channel 400 GHz were placed at different angles of rotations. The AWG devices were rotated at  $0^\circ$ ,  $15^\circ$ ,  $30^\circ$ ,  $45^\circ$ ,  $77^\circ$  and  $90^\circ$  as shown in Fig. 7(a). Extracted insertion loss and crosstalk levels from the measurements are plotted in Fig. 7(b). As we can see, no clear trend can be observed in the plot. This absence of trend could be attributed to changing of grid size from 5 nm to 1 nm, but also on the use of different photoresist, different illumination wavelength, and possibly different mask writing strategies. The key conclusion is that, with the technological progress of the past decade, the problem of rotated waveguides is no longer a major concern.

In the same exercise we also performed a small study of the propagation losses of waveguides oriented at different angles. Waveguide spirals of 5 cm length were also placed at 5 different angles of  $0^\circ$ ,  $15^\circ$ ,  $30^\circ$ ,  $45^\circ$  and  $77^\circ$  to find out the effect of rotation on the losses of waveguides. Rotated waveguide spirals and the measured transmission responses are shown in Fig. 8. It can be noticed in the plot that there is no noticeable difference in transmission for different rotations of the waveguide spirals. We do see that the transmission spectrum of the long waveguides exhibits substantial 'noise'. The rapid fluctuations are not an artifact of the measurements, but are deterministic. They originate in backscattering of light in the waveguides, which creates a multitude of interferences that result in a wavelength dependent transmission.<sup>26</sup>

## 5. WAFER LEVEL TREND

We measured the devices over an entire wafer to find out the wafer-level trends for the performance parameters like insertion loss, cross-talk, next neighbor cross-talk and the deviation from the designed wavelength. Wafer maps of performance parameters for devices with 50  $\mu\text{m}$  extra length and 450 nm linewidth are shown in Fig. 9. It can be noticed in Fig. 9(a) that insertion loss is uniform over the wafer with some exceptions at the edges. The average channel wavelength deviation over the wafer is shown in Fig. 9(b), and we see that the deviation from

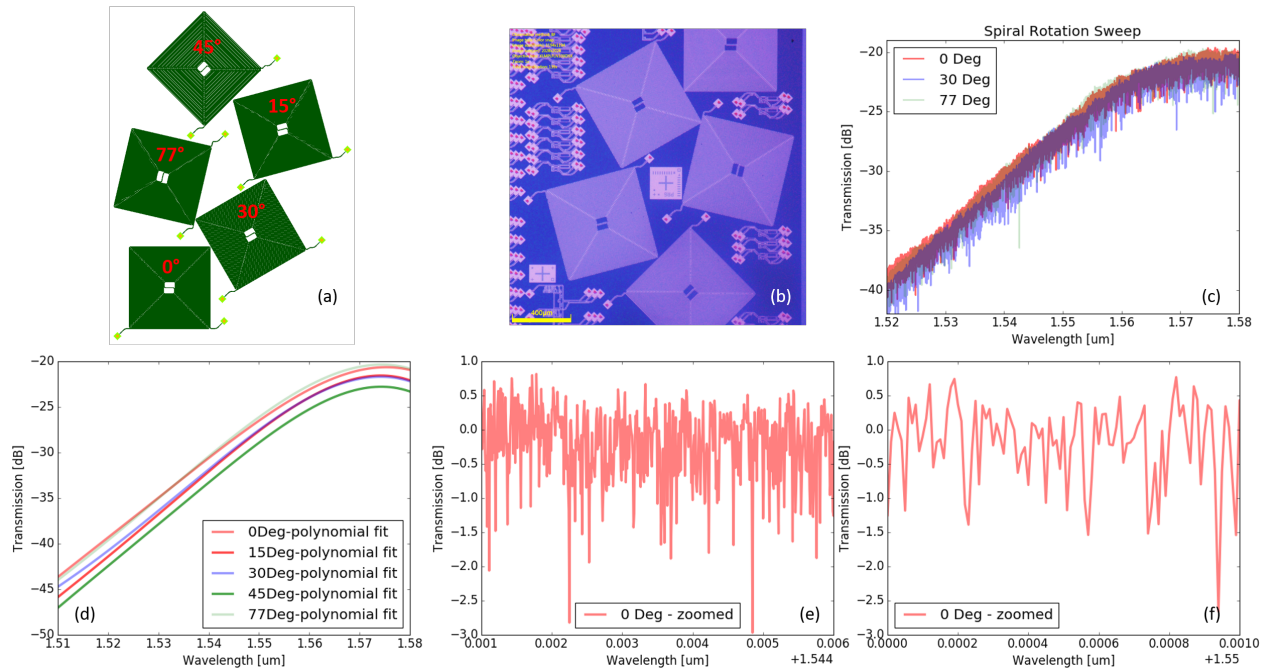


Figure 8. (a) A snippet from the GDSII explaining the rotation of the waveguide spirals at different angles. (b) Microscope image showing spirals at different angles of rotations. (c) Measured transmission responses are plotted for  $0^\circ$ ,  $30^\circ$  and  $77^\circ$  rotated spirals to show that transmission does not change significantly. (d) Plot showing the 4th order polynomial fit to the measured transmission responses for different rotations of the spirals. (e) Transmission response for the spiral without any rotation i.e.  $0^\circ$  is shown for a small wavelength span. It should be mentioned here that transmission is being normalized to the respective polynomial fit. (f) Zoomed transmission response to show the fluctuations.

the desired wavelength is minimum at the center of the wafer, and increases towards the edges in an annular way. This can be related to variations in effective index, which in turn is related to the waveguide width and thickness.<sup>27</sup> The thickness of the silicon layer also varies in a similar way due to the polishing effect, and many plasma etch tools also have some radial nonuniformity of plasma composition. Average channel cross-talks and next neighbour cross-talk values are shown in Fig. 9(c) and Fig. 9(d), respectively. We do observe some small islands in the cross-talk wafer map which can be attributed to the local die-level width variations as thickness is a wafer level phenomenon, or even random coincidences of phase errors that amount to constructive interference.

## 6. CONCLUSIONS

In this paper we presented a study of how design parameters in AWGs can affect the performance in high-contrast silicon photonic circuits. In particular, we looked into the effect of the average length of the delay lines by adding additional length to all delay lines without otherwise changing the AWG layout. This shows, as expected, that the additional length does degrade the performance. Similarly, we made the delay lines wider to reduce the sensitivity to small linewidth variations, and we corroborated previously demonstrated trends that the phase errors decrease and the performance metrics of the AWGs improve as we make the waveguides wider. We also reproduced an earlier study of rotated AWG layouts to quantify the effect of mask discretisation on the performance. Here, we found that improvements in the technology made the earlier observed degradation at different angles disappear. This was also confirmed with the loss measurements in waveguide spirals, where there was no noticeable dependence of the transmission on the angle in the layout.

## ACKNOWLEDGMENTS

Part of this work is supported by the Flemish Research Foundation (FWO-Vlaanderen) with grant G013815N. Part of this work is supported by the Flemish Agency for Innovation and Entrepreneurship (VLAIO) with the MEPIC project.

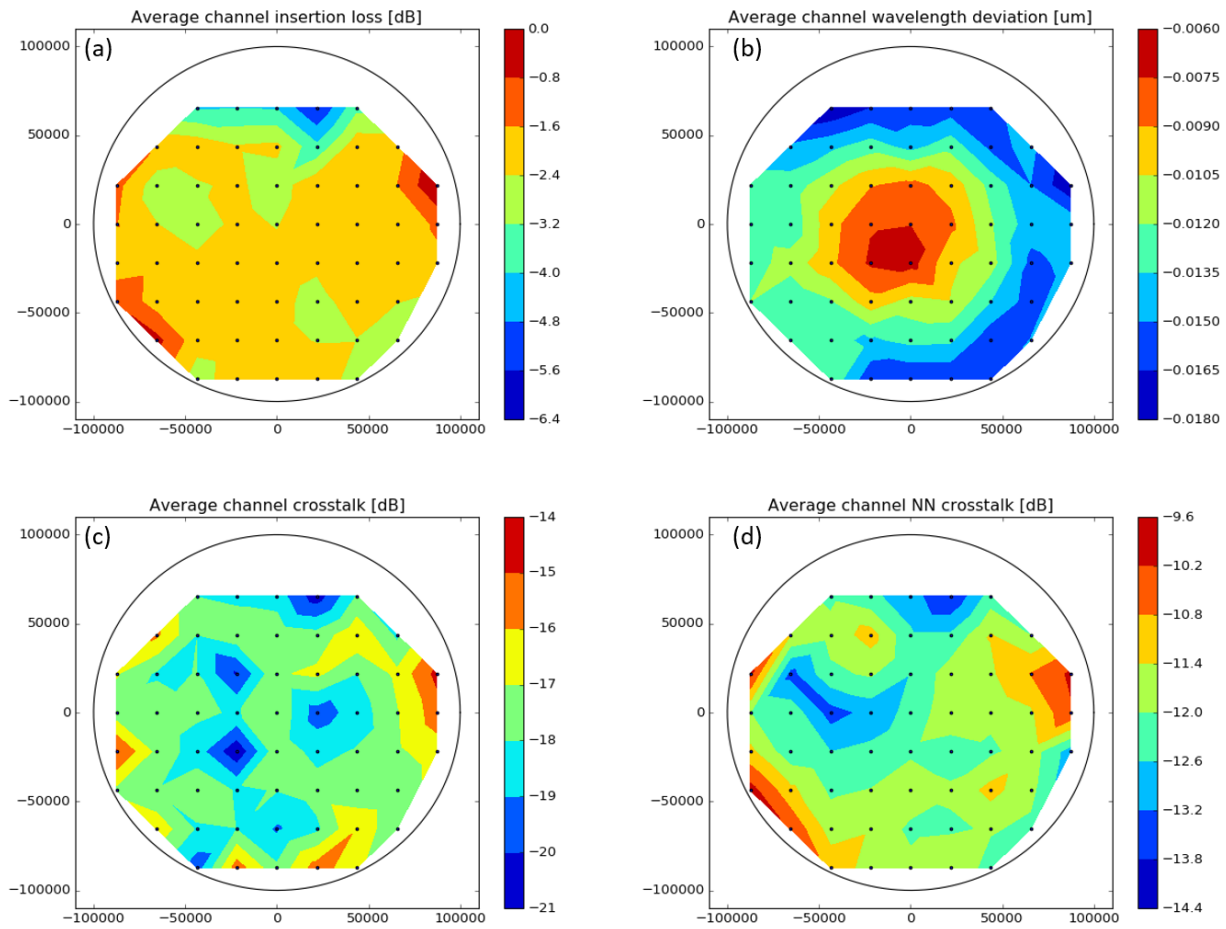


Figure 9. Wafer level trends for 8 channel 400GHz devices having an extra length of  $50 \mu\text{m}$  are plotted. (a) Extracted channel insertion loss over the wafer. (b) Extracted channel wavelength deviation over the wafer. (c) Extracted channel crosstalk over the wafer. (d) Extracted next neighbour crosstalk over the wafer.

## REFERENCES

- [1] Khan, M. U., Xing, Y., Ye, Y., and Bogaerts, W., “Photonic integrated circuit design in a foundry+fabless ecosystem,” *IEEE Journal of Selected Topics in Quantum Electronics* **25**, 1–14 (Sep. 2019).
- [2] Selvaraja, S. K., Bogaerts, W., Dumon, P., Van Thourhout, D., and Baets, R., “Subnanometer linewidth uniformity in silicon nanophotonic waveguide devices using CMOS fabrication technology,” *IEEE Journal on Selected Topics in Quantum Electronics* **16**(1), 316–324 (2010).
- [3] Dragone, C., “An N X N optical multiplexer using a planar arrangement of 2 star couplers,” *IEEE Phot. Techn. Lett.* **3**(9), 812–815 (1991).
- [4] Smit, M., “New focusing and dispersive planar component based on an optical phased array,” *Electronics Letters* **24**(7), 385 (1988).
- [5] Doerr, C. R., “Planar Lightwave Devices for WDM,” in [*Optical Fiber Telecommunications*], Kaminow, I. P. and Li, T., eds., **IV A**, ch. 9, 405–476, Academic Press, ISBN 0-12-395172-0 (2002).
- [6] Claes, T., Bogaerts, W., and Bienstman, P., “Experimental characterization of a silicon photonic biosensor consisting of two cascaded ring resonators based on the Vernier-effect and introduction of a curve fitting method for an improved detection limit,” *Optics Express* **18**(22), 22747 (2010).
- [7] Subramanian, A. Z., Ryckeboer, E., Dhakal, A., Peyskens, F., Malik, A., Kuyken, B., Zhao, H., Pathak, S., Ruocco, A., De Groote, A., et al., “Silicon and silicon nitride photonic circuits for spectroscopic sensing on-a-chip,” *Photonics Research* **3**(5), B47–B59 (2015).
- [8] Park, J., Joo, J., Kim, G., Yoo, S.-W., and Kim, S., “Low-crosstalk silicon nitride arrayed waveguide grating for the 800-nm band,” *IEEE Photonics Technology Letters* **31**(14), 1183–1186 (2019).
- [9] Acoleyen, K. V., Bogaerts, W., and Baets, R., “Two-Dimensional Dispersive Off-Chip Beam Scanner,” *IEEE Photon Technol. Lett.* **23**(17), 1270–1272 (2011).
- [10] Pantouvaki, M., Srinivasan, S. A., Ban, Y., De Heyn, P., Verheyen, P., Lepage, G., Chen, H., De Coster, J., Golshani, N., Balakrishnan, S., Absil, P., and Van Campenhout, J., “Active Components for 50 Gb/s NRZ-OOK Optical Interconnects in a Silicon Photonics Platform,” *Journal of Lightwave Technology* **35**(4), 631–638 (2017).
- [11] Bogaerts, W., Dumon, P., Van Thourhout, D., Taillaert, D., Jaenen, P., Wouters, J., Beckx, S., Wiaux, V., and Baets, R. G., “Compact wavelength-selective functions in silicon-on-insulator photonic wires,” *IEEE Journal on Selected Topics in Quantum Electronics* **12**, 1394–1401 (12 2006).
- [12] Bogaerts, W., Selvaraja, S. K., Dumon, P., Brouckaert, J., De Vos, K., Van Thourhout, D., and Baets, R., “Silicon-on-insulator spectral filters fabricated with CMOS technology,” *IEEE Journal on Selected Topics in Quantum Electronics* **16**(1), 33–44 (2010).
- [13] Bock, P., Cheben, P., Schmid, J., Xu, D.-X., Janz, S., and Hall, T., “Sub-wavelength grating gradient index mode transformers in high index contrast slab waveguides,” in [*Silicon Photonics IV*], **7220**, 722005, International Society for Optics and Photonics (2009).
- [14] Goh, T., Suzuki, S., and Sugita, A., “Estimation of waveguide phase error in silica-based waveguides,” *Journal of Lightwave Technology* **15**(11), 2107–2113 (1997).
- [15] Dumon, P., Priem, G., Nunes, L. R., Bogaerts, W., Van Thourhout, D., Bienstman, P., Liang, T. K., Tsuchiya, M., Jaenen, P., Beckx, S., Wouters, J., and Baets, R., “Linear and nonlinear nanophotonic devices based on silicon-on-insulator wire waveguides,” *Japanese Journal of Applied Physics, Part 1: Regular Papers and Short Notes and Review Papers* **45**, 6589–6602 (8 2006).
- [16] Pathak, S., Vanslebrouck, M., Dumon, P., Van Thourhout, D., Verheyen, P., Lepage, G., Absil, P., and Bogaerts, W., “Effect of mask discretization on performance of silicon arrayed waveguide gratings,” *IEEE Photonics Technology Letters* **26**(7), 718–721 (2014).
- [17] Pathak, S., Dumon, P., Van Thourhout, D., and Bogaerts, W., “Comparison of AWGs and Echelle Gratings for Wavelength Division Multiplexing on Silicon-on-Insulator,” *IEEE Photonics Journal* **6**, 1–9 (10 2014).
- [18] Bogaerts, W., Xing, Y., and Khan, U., “Layout-aware variability analysis, yield prediction, and optimization in photonic integrated circuits,” *IEEE Journal of Selected Topics in Quantum Electronics* **25**, 1–13 (Sep. 2019).
- [19] Xing, Y., Dong, J., Dwivedi, S., Khan, U., and Bogaerts, W., “Accurate extraction of fabricated geometry using optical measurement,” *Photonics Research* **6**(11), 1008 (2018).

- [20] Khan, U., Xing, Y., and Bogaerts, W., “Parameter extraction, variability analysis and yield prediction of the photonic integrated circuits,” in [*Integrated Photonics Research, Silicon and Nanophotonics*], IM3A–2, Optical Society of America (2019).
- [21] Xing, Y., Dong, J., Khan, U., and Bogaerts, W., “Hierarchical Model for Spatial Variations of Integrated Photonics,” *IEEE International Conference on Group IV Photonics*, 91–92 (2018).
- [22] Khan, U., Xing, Y., and Bogaerts, W., “Effect of fabrication imperfections on the performance of silicon-on-insulator arrayed waveguide gratings,” in [*IEEE Photonics Benelux Chapter/Annual Symposium 2018*], 1–5 (2018).
- [23] Pathak, S., Van Thourhout, D., and Bogaerts, W., “Design trade-offs for silicon-on-insulator-based AWGs for (de)multiplexer applications,” *Optics Letters* **38**, 2961 (8 2013).
- [24] Dumon, P., [*Ultra-compact integrated optical filters in silicon-on-insulator by means of wafer-scale technology*], PhD Thesis, Ghent University (2007).
- [25] Bogaerts, W. and Li, Y., “Integrated design for integrated photonics: from the physical to the circuit level and back,” *SPIE Optics+Photonics* **8781**, 878102–878102 (2013).
- [26] Li, A., Xing, Y., Van Laer, R., Baets, R., and Bogaerts, W., “Extreme spectral transmission fluctuations in silicon nanowires induced by backscattering,” in [*2016 IEEE 13th International Conference on Group IV Photonics (GFP)*], 160–161, IEEE (2016).
- [27] Xing, Y., Dong, J., Dwivedi, S., Khan, U., and Bogaerts, W., “Accurate Extraction of Fabricated Geometry Using Optical Measurement,” *Photonics Research* **6**(11), 1008–1020 (2018).